

Universal Weakly Fault-Tolerant Quantum Computation via Code Switching in the $[[8,3,2]]$ Code

Shixin Wu,^{1,2} Dawei Zhong,^{2,3} Todd A. Brun,^{1,2,3,4} and Daniel A. Lidar^{1,2,3,5,6}

¹*Department of Electrical & Computer Engineering,
University of Southern California, Los Angeles, California 90089, USA*

²*Center for Quantum Information Science & Technology,
University of Southern California, Los Angeles, CA 90089, USA*

³*Department of Physics & Astronomy, University of Southern California, Los Angeles, California 90089, USA*

⁴*Department of Computer Science, University of Southern California, Los Angeles, California 90089, USA*

⁵*Department of Chemistry, University of Southern California, Los Angeles, California 90089, USA*

⁶*Quantum Elements, Inc., 2829 Townsgate Road, Westlake Village, CA, 91361, USA*

Code-switching offers a route to universal, fault-tolerant quantum computation by circumventing the limitation implied by the Eastin-Knill theorem against a universal transversal gate set within a single quantum code. Here, we present a fault-tolerant code-switching protocol between two versions of the $[[8, 3, 2]]$ code. One version supports weakly fault-tolerant single-qubit Clifford gates, while the other supports a logical $\overline{\text{CCZ}}$ gate via transversal T/T^\dagger together with logical $\overline{\text{CZ}}$, CNOT, and SWAP gates. Because both codes have distance 2, the protocol operates in a postselected, error-detecting regime: single faults lead to detectable outcomes, and accepted runs exhibit quadratic suppression of logical error rates. This yields a universal scheme for postselected fault-tolerant computation. We validate the protocol numerically through simulations of state preparation, code switching, and a three-logical-qubit implementation of Grover’s search.

I. INTRODUCTION

Quantum error correction (QEC) protects quantum information from noise by encoding logical states into a codespace, i.e., a subspace of the full physical Hilbert space [1–7]. Beyond storage, quantum computation also requires controlled processing of encoded logical information. This is accomplished by applying quantum circuits that transform logical states while preserving the codespace. Moreover, these circuits must be *fault-tolerant*: errors must not spread faster than the code’s ability to correct them, or, for distance-2 codes, at least to detect them. When this condition is met for a suitable choice of code and for physical error rates below a threshold, the logical error rate can be suppressed to an arbitrarily low value for an arbitrarily long computation [8–12].

One of the simplest routes to fault tolerance is through *transversal* gate implementations [13]. A transversal logical gate decomposes into physical gates that act independently on each qubit within a code block (and, for two-block gates, couple only corresponding qubits across blocks). This structure prevents a single physical error from spreading within a block and turning into a higher-weight error [11, 14]. While scaling quantum computers to fully error-correcting fault tolerance remains challenging, a recent study demonstrated an approach to *weak* fault tolerance in implementing the logical Clifford set on the $[[n, n - 2, 2]]$ family of codes without using any transversal logical gates [15]. In this weakly fault-tolerant setting, circuits are designed so that any error produced by a single faulty gate or measurement is detectable by measuring ancillas used in their weakly fault-tolerant circuits that implement two-qubit entangling gates. Runs with nontrivial syn-

drome are discarded [11, 15]. Although this approach is error-detecting rather than error-correcting, postselection yields a quadratic suppression of logical errors, consistent with the expected behavior of the high-rate $[[n, n - 2, 2]]$ family of codes, and does not require real-time decoding and feedback.

Encoded universal quantum computation requires a set of logical gates that can approximate any unitary transformation [16]. A common minimal choice is $\{H, \text{CNOT}, T\}$ [17]. However, the Eastin-Knill theorem implies that no QEC code admits a universal set of *transversal* logical gates [14]. A widely used workaround is magic-state injection and distillation [18]: noisy “magic states” are injected as non-Clifford resources, and distillation (using only Clifford operations) converts many noisy copies into fewer copies with higher fidelity. However, estimates indicate that realizing a single high-fidelity logical T gate can require on the order of 10^3 code cycles [19], which remains far beyond the reach of many near-term platforms.

An alternative route to a fault-tolerant universal gate set is *code switching* between codes that implement complementary logical gates via transversal physical gates [20]. Switching codes while preserving the logical information typically proceeds via *gauge fixing*, i.e., measuring suitable gauge operators and projecting onto eigenstates so that the measured eigenoperators become stabilizer generators of the target code [21–24].

Fault-tolerant code-switching protocols have been developed, for example, between the $[[7, 1, 3]]$ Steane code (the smallest 2D color code) and the $[[15, 1, 3]]$ Reed-Muller code (the smallest 3D color code) [20, 24]. The same work also presented a protocol between the $[[7, 1, 3]]$ Steane code and a “morphed” $[[10, 1, 2]]$ code derived from the $[[15, 1, 3]]$ Reed-Muller code [25], reducing cir-

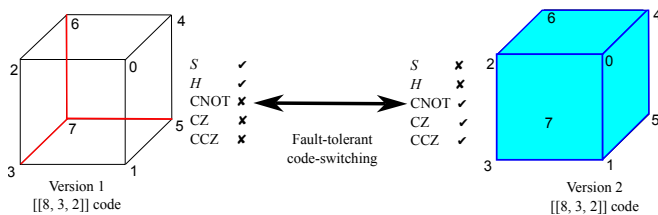


FIG. 1. Summary of this work. The two versions of the $[[8, 3, 2]]$ code, each of which can be geometrically represented by a cube. The three red edges of the $[[8, 3, 2]]_1$ code represent the fixed weight-2 gauge G^X operators, and the three blue faces of the $[[8, 3, 2]]_2$ code represent the fixed weight-4 gauge G^Z operators.

cuit depth and resource requirements, at the cost of reduced error-correction capability.

In this work, we further reduce the required resources by code switching between two versions of the $[[8, 3, 2]]$ code. Because our codes have distance 2, we adopt fault tolerance in the error-detecting (postselected) sense. One version of the $[[8, 3, 2]]$ code is the “smallest interesting color code,” with fault-tolerant implementations of the logical CCZ, CZ, and CNOT gates [26–30]. We call this the *Version 2* $[[8, 3, 2]]$ code, because it lacks fault-tolerant implementations of logical single-qubit gates. The *Version 1* $[[8, 3, 2]]$ code can instead use the weakly fault-tolerant circuits of Ref. [15] to implement the logical H , S , and \sqrt{X}^\dagger gates. Together, the two codes provide an overcomplete universal set of logical gates while still achieving quadratic suppression of logical errors with postselection. This protocol is summarized in Fig. 1.

The remainder of the paper is organized as follows. We first review, in Section II, the weakly fault-tolerant logical gates available on the $[[n, n-2, 2]]$ family. Then, in Section III, we introduce our two versions of the $[[8, 3, 2]]$ code. In Section IV, we present a fault-tolerant code-switching protocol between them. Next, in Section V, we construct fault-tolerant state-preparation circuits for logical states relevant to applications. Finally, in Section VI, we report numerical simulations of state preparation, code switching, and an encoded three-logical-qubit Grover search. The Appendix presents various technical details in support of the main text.

II. FAULT-TOLERANT LOGICAL GATES ON $[[n, n-2, 2]]$ CODES

This section summarizes the constructions in [15] for implementing weakly fault-tolerant logical single-qubit gates (H , S , and \sqrt{X}^\dagger) on the $[[n, n-2, 2]]$ code family with two-qubit entangling gates. Since these codes have distance $d=2$, our notion of fault tolerance is the $d=2$, postselected one: any single fault during the circuit must either leave the data in the codespace or produce an error that is detected by the stabilizer (and ancilla) measure-

ments, so that the run can be discarded.

The $[[n, n-2, 2]]$ code has stabilizer generators

$$S_X = X^{\otimes n}, \quad S_Z = Z^{\otimes n}. \quad (1)$$

A convenient choice of logical Pauli operators is

$$\bar{X}_j = X_j X_{n-2}, \quad \bar{Z}_j = Z_j Z_{n-1} \quad (j = 0, \dots, n-3), \quad (2)$$

with $\bar{Y}_j \equiv i\bar{X}_j\bar{Z}_j$ (global phases are irrelevant throughout).

Logical gates implemented *transversally* are naturally compatible with weak fault tolerance: a single faulty location can create at most a weight-1 error in each code block, which remains detectable for a distance-2 code. By contrast, entangling gates that act *within* a block can spread a single fault to multiple data qubits, producing higher-weight errors. Such gates can still be used in a weakly fault-tolerant manner, but only when embedded in ancilla-assisted measurement gadgets that ensure any single fault produces a detectable syndrome.

It is useful to distinguish three conceptual levels:

$$\text{Logical level} \rightarrow \text{Physical level} \rightarrow \text{FT physical level}. \quad (3)$$

At the *logical level*, we denote ideal encoded operations with a straight overline (e.g., \bar{H}_j). At the *physical level*, we write the corresponding compilation into elementary two-qubit rotations with a wavy overline (e.g., $\widetilde{XX}(i, j)$). These physical-level two-qubit entangling gates are not fault-tolerant on a distance-2 code and must be replaced by fault-tolerant gadgets at the *FT physical level*; the gadgets we use are shown in Section A. We write products of unitaries in the usual right-to-left circuit order (the rightmost factor acts first).

A. Elementary Clifford rotations

Both the physical-level compilation and the FT gadgets use the following Clifford rotations:

$$U_{XX} := \frac{I + iXX}{\sqrt{2}}, \quad U_{YY} := \frac{I - iYY}{\sqrt{2}}, \quad (4a)$$

$$U_{ZZ} := \frac{I - iZZ}{\sqrt{2}}, \quad R_X := \frac{I - iX}{\sqrt{2}}, \quad (4b)$$

where XX , YY , and ZZ denote products of Pauli operators on two qubits (e.g., $XX = X \otimes X$). We refer to these as the XX , YY , ZZ , and R_X gates; note the opposite sign convention for the XX gate. We use $\widetilde{XX}(i, j)$ (resp. $\widetilde{ZZ}(i, j)$) to denote applying U_{XX} (resp. U_{ZZ}) to physical qubits i and j .

For later reference, Table I lists the conjugation action of the XX and ZZ rotations on a set of two-qubit Pauli operators used in the discussion.

	XI	ZI	YX	YZ	XX	ZZ
XX gate	XI	YX	$-ZI$	YZ	XX	ZZ
ZZ gate	YZ	ZI	YX	$-XI$	XX	ZZ

TABLE I. Conjugation action of the XX and ZZ rotation gates on selected two-qubit Pauli operators (e.g., XI denotes $X \otimes I$). Other Pauli mappings follow analogously.

B. Logical level \rightarrow Physical level

At the physical level, the logical single-qubit gates \bar{S}_j , $\sqrt{\bar{X}}_j^\dagger$, and \bar{H}_j can be expressed using \widetilde{XX} and \widetilde{ZZ} rotations involving the “shared” qubits $n-2$ and $n-1$:

$$\bar{S}_j = \widetilde{ZZ}(j, n-1), \quad \sqrt{\bar{X}}_j^\dagger = \widetilde{XX}(j, n-2), \quad (5)$$

and

$$\bar{H}_j = \widetilde{XX}(j, n-2) \widetilde{ZZ}(j, n-1) \widetilde{XX}(j, n-2) Y_j \widetilde{X}_{n-2} \widetilde{Z}_{n-1}. \quad (6)$$

The final factor $Y_j \widetilde{X}_{n-2} \widetilde{Z}_{n-1}$ is a *Pauli byproduct correction* (not merely a global phase). The sequence $\widetilde{XX} \cdot \widetilde{ZZ} \cdot \widetilde{XX}$ implements \bar{H}_j up to a known logical \bar{Y}_j correction, and with our choice of logical operators,

$$\bar{Y}_j \equiv Y_j X_{n-2} Z_{n-1} \quad (7)$$

up to an irrelevant phase.

The identities above follow from Table I together with the standard single-qubit Clifford conjugation rules

$$\begin{aligned} SX S^\dagger &= Y, & SY S^\dagger &= -X, & SZ S^\dagger &= Z, \\ \sqrt{\bar{X}}^\dagger X \sqrt{\bar{X}} &= X, & \sqrt{\bar{X}}^\dagger Y \sqrt{\bar{X}} &= -Z, & \sqrt{\bar{X}}^\dagger Z \sqrt{\bar{X}} &= Y, \\ HXH &= Z, & HYH &= -Y, & HZH &= X. \end{aligned} \quad (8)$$

For example, $\widetilde{ZZ}(j, n-1)$ leaves \bar{Z}_j invariant and maps $\bar{X}_j \mapsto \bar{Y}_j$ (up to phase), matching the action of \bar{S}_j . Similarly, $\widetilde{XX}(j, n-2)$ leaves \bar{X}_j invariant and maps $\bar{Z}_j \mapsto \bar{Y}_j$, matching the action of $\sqrt{\bar{X}}_j^\dagger$.

C. Physical level \rightarrow FT physical level

The two-qubit entangling gates \widetilde{XX} and \widetilde{ZZ} are not automatically fault-tolerant on a distance-2 code, because they may produce weight-2 errors on the data qubits that are logical errors in most cases. Because the probabilities for two-qubit entangling gates to produce weight-1 and weight-2 errors are both on the order of $O(p)$, where p is the error probability of the gate, logical errors cannot be quadratically suppressed. Ref. [15] replaces each $\widetilde{XX}(j, n-2)$ and $\widetilde{ZZ}(j, n-1)$ by an ancilla-assisted, verification/postselection gadget that is fault-tolerant in the error-detecting sense where all two-qubit

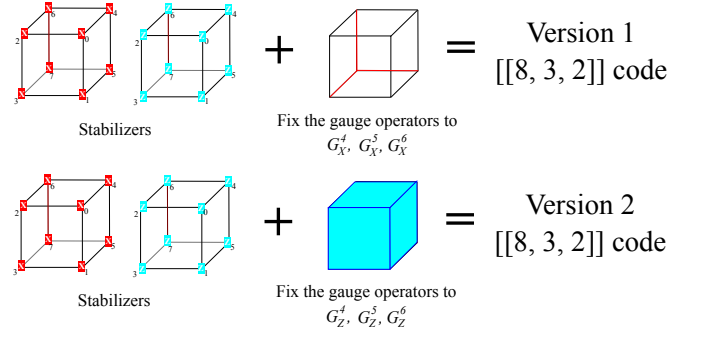


FIG. 2. Obtaining the two versions of the $[[8, 3, 2]]$ code by fixing the gauge operators of the $[8, 3, 3, 2]$ subsystem code. Combining with the transversal $X^{\otimes 8}$ and $Z^{\otimes 8}$ stabilizers of the $[[8, 3, 3, 2]]$ subsystem code, fixing the gauge operators give the different stabilizers that define the two stabilizer $[[8, 3, 2]]$ codes.

entangling gates act on a data qubit and an ancilla and none on two data qubits. We reproduce these gadgets in Section A (Figs. 9 and 10) and use them as primitives in the remainder of this paper.

III. TWO VERSIONS OF THE $[[8, 3, 2]]$ CODE

In this section, we discuss two versions of the $[[8, 3, 2]]$ stabilizer code: the Version 1 $[[8, 3, 2]]$ code ($[[8, 3, 2]]_1$) and the Version 2 $[[8, 3, 2]]$ code ($[[8, 3, 2]]_2$), as well as their construction from the $[[8, 6, 2]]$ code. The constructions of the two versions are summarized in Fig. 2.

A. Subsystem $[[8, 3, 3, 2]]$ code

The subsystem $[[8, 3, 3, 2]]$ code is constructed from the $[[8, 6, 2]]$ stabilizer code by “gauging out” three of its six logical operators. The stabilizers of the $[[8, 6, 2]]$ codes are $X^{\otimes 8}$ and $Z^{\otimes 8}$. We then choose the following logical operators, which differ from the canonical all-weight-2 choice. This choice is crucial for the code-switching protocol to function, and corresponds to changing the basis of the codespace.

$$\begin{aligned} \bar{X}_1 &= X_0 X_1 X_2 X_3, & \bar{Z}_1 &= Z_0 Z_4 \\ \bar{X}_2 &= X_0 X_1 X_4 X_5, & \bar{Z}_2 &= Z_0 Z_2 \\ \bar{X}_3 &= X_0 X_2 X_4 X_6, & \bar{Z}_3 &= Z_0 Z_1 \\ G_4^X &= X_7 X_3, & G_4^Z &= Z_0 Z_1 Z_2 Z_3 \\ G_5^X &= X_7 X_5, & G_5^Z &= Z_0 Z_1 Z_4 Z_5 \\ G_6^X &= X_7 X_6, & G_6^Z &= Z_0 Z_2 Z_4 Z_6 \end{aligned} \quad (9)$$

Gauging out the last three logical qubits—that is, not using them to store logical data and not requiring that they be protected—gives us the $[[8, 3, 3, 2]]$ subsystem code. We refer to the last three logical qubits as “gauge qubits”

and their corresponding logical operators as “gauge operators.”

B. The $[[8, 3, 2]]_1$ stabilizer code

Version 1 of the $[[8, 3, 2]]$ stabilizer code is obtained by fixing the gauge qubits of the $[[8, 3, 3, 2]]$ code into the logical $|\overline{\uparrow}\rangle$ state. This means the logical X operators of the three gauge qubits now become stabilizers of the code. The new set of stabilizer generators is

$$X^{\otimes 8}, Z^{\otimes 8}, X_7X_3, X_7X_5, X_7X_6. \quad (10)$$

The additional X stabilizer generators reduce the first three logical operators to weight-2:

$$\begin{aligned} \overline{X}_1 &= X_0X_1X_2X_3 \cdot X^{\otimes 8} \cdot X_7X_5 = X_6X_4, \\ \overline{X}_2 &= X_0X_1X_4X_5 \cdot X^{\otimes 8} \cdot X_7X_3 = X_6X_2, \\ \overline{X}_3 &= X_0X_2X_4X_6 \cdot X^{\otimes 8} \cdot X_3X_5X_7X_6 = X_6X_1. \end{aligned} \quad (11)$$

Its logical Z operators remain unchanged:

$$\overline{Z}_1 = Z_0Z_4, \quad \overline{Z}_2 = Z_0Z_2, \quad \overline{Z}_3 = Z_0Z_1. \quad (12)$$

Note that the logical operators are similar to those used in [15], in that all of them are weight-2 (instead of a mix of weight-4 and weight-2 in our original choice) and that the shared qubits for the logical \overline{X} and \overline{Z} operators are unique for different logical qubits. As a result, we can use

the same construction as in Section II to implement the logical \overline{H} , \overline{S} , and $\sqrt{\overline{X}^\dagger}$ gates for the Version 1 $[[8, 3, 2]]$ code:

$$\begin{aligned} \overline{H}_1 &= \widetilde{ZZ}(4, 0) \cdot \widetilde{XX}(4, 6) \cdot \widetilde{ZZ}(4, 0) \cdot Y_4X_6Z_0, \\ \overline{H}_2 &= \widetilde{ZZ}(2, 0) \cdot \widetilde{XX}(2, 6) \cdot \widetilde{ZZ}(2, 0) \cdot Y_2X_6Z_0, \\ \overline{H}_3 &= \widetilde{ZZ}(1, 0) \cdot \widetilde{XX}(1, 6) \cdot \widetilde{ZZ}(1, 0) \cdot Y_1X_6Z_0. \end{aligned} \quad (13)$$

$$\begin{aligned} \overline{S}_1 &= \widetilde{ZZ}(4, 0), \quad \sqrt{\overline{X}^\dagger}_1 = \widetilde{XX}(4, 6), \\ \overline{S}_2 &= \widetilde{ZZ}(2, 0), \quad \sqrt{\overline{X}^\dagger}_2 = \widetilde{XX}(2, 6), \\ \overline{S}_3 &= \widetilde{ZZ}(1, 0), \quad \sqrt{\overline{X}^\dagger}_3 = \widetilde{XX}(1, 6). \end{aligned} \quad (14)$$

Then, we use the fault-tolerant implementation of Fig. 9 and Fig. 10 to replace \widetilde{XX} and \widetilde{ZZ} . Finally, logical SWAPs among the three encoded qubits are induced by the corresponding permutations of the physical qubits $\{1, 2, 4\}$, since these are the qubits that distinguish the three logical-qubit labels. On hardware platforms that permit software reassignment of qubit identities, these operations can be treated as qubit permutations rather than as explicit logical gate sequences. On fixed-layout architectures, the same permutations would need to be realized by explicit SWAP networks or qubit motion.

Although a fault-tolerant implementation of the logical in-block CNOT gate is also proposed in [15], we decide not to use it in the Version 1 $[[8, 3, 2]]$ code because of its large circuit depth. Rather, CNOTs can be easily implemented in Version 2, as we will see in the next section.

C. The $[[8, 3, 2]]_2$ stabilizer code

Version 2 of the $[[8, 3, 2]]$ stabilizer code is obtained by fixing the gauge qubits of the $[[8, 3, 3, 2]]$ code in the logical $|\overline{0}\rangle$ state. This means that the logical Z operators of the gauge qubits now become stabilizer generators for the code. The new set of stabilizer generators is

$$X^{\otimes 8}, Z^{\otimes 8}, Z_0Z_1Z_2Z_3, Z_0Z_1Z_4Z_5, Z_0Z_2Z_4Z_6. \quad (15)$$

This recovers the $[[8, 3, 2]]$ code (version 2) that allows a fault-tolerant logical CCZ gate with transversal T and T^\dagger gates [26]:

$$\overline{CCZ} = T_0T_1^\dagger T_2^\dagger T_3T_4^\dagger T_5T_6T_7^\dagger. \quad (16)$$

In addition, this code also allows fault-tolerant implementations of the logical CZ , SWAP, in-block CNOT gates, and inter-block CNOT gates [27–30]. The logical CZ gates are implemented with phase gates:

$$\begin{aligned} \overline{CZ}(1, 2) &= S_0S_2^\dagger S_4^\dagger S_6, \\ \overline{CZ}(1, 3) &= S_0S_1^\dagger S_4^\dagger S_5, \\ \overline{CZ}(2, 3) &= S_0S_1^\dagger S_2^\dagger S_3. \end{aligned} \quad (17)$$

The logical SWAP gates are implemented by cyclic-permuting the physical qubits:

$$\begin{aligned} \overline{SWAP}(1, 2) &: 0 \rightarrow 4 \rightarrow 6 \rightarrow 2 \rightarrow 0, \quad 1 \rightarrow 5 \rightarrow 7 \rightarrow 3 \rightarrow 1, \\ \overline{SWAP}(1, 3) &: 2 \rightarrow 6 \rightarrow 7 \rightarrow 3 \rightarrow 2, \quad 0 \rightarrow 4 \rightarrow 5 \rightarrow 1 \rightarrow 0, \\ \overline{SWAP}(2, 3) &: 0 \rightarrow 2 \rightarrow 3 \rightarrow 1 \rightarrow 0, \quad 4 \rightarrow 6 \rightarrow 7 \rightarrow 5 \rightarrow 4. \end{aligned} \quad (18)$$

Similarly, these physical SWAP operations can be treated either as qubit permutations or as explicit qubit motions, depending on the layout of different architectures.

Likewise, the following in-block logical CNOT gates are induced by physical-qubit permutations:

$$\begin{aligned} \overline{CNOT}(1, 2) &= 0 \leftrightarrow 4, 1 \leftrightarrow 5, \quad \overline{CNOT}(2, 1) = 0 \leftrightarrow 2, 1 \leftrightarrow 3 \\ \overline{CNOT}(1, 3) &= 0 \leftrightarrow 4, 2 \leftrightarrow 6, \quad \overline{CNOT}(3, 1) = 0 \leftrightarrow 1, 2 \leftrightarrow 3 \\ \overline{CNOT}(2, 3) &= 0 \leftrightarrow 2, 4 \leftrightarrow 6, \quad \overline{CNOT}(3, 2) = 0 \leftrightarrow 1, 4 \leftrightarrow 5 \end{aligned} \quad (19)$$

D. Block-scalability

We consider scaling up with blocks of the $[[8, 3, 2]]$ code, which requires performing entangling gates between logical qubits in different blocks.

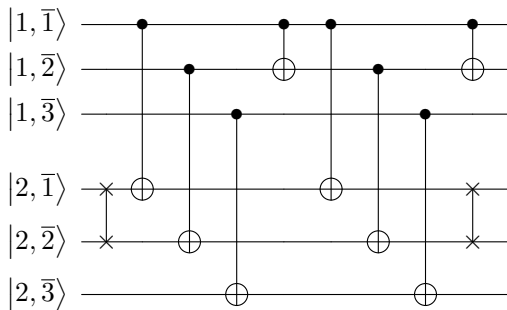


FIG. 3. The logical circuit for the single-pair inter-block $\overline{\text{CNOT}}$ from logical qubit $\bar{1}$ of block 1 to logical qubit $\bar{1}$ of block 2 [27]. If the two logical SWAP gates are omitted, the circuit instead implements $\text{CNOT}(|1, \bar{1}\rangle, |2, \bar{2}\rangle)$; the SWAPs simply swaps the target from $|2, \bar{2}\rangle$ to $|2, \bar{1}\rangle$. Variants of this construction are given in Section C.

A parallel inter-block logical $\overline{\text{CNOT}}$ gate means that the transversal physical CNOT gates applied between corresponding qubits of two code blocks, so that the three corresponding logical qubits undergo logical $\overline{\text{CNOT}}$ gates in parallel. When the two blocks are in the same version of the $[[8, 3, 2]]$ code, this transversal CNOT preserves the CSS stabilizer structure and therefore defines a valid encoded operation. For mixed versions, the situation is asymmetric. If the control block is $[[8, 3, 2]]_1$ and the target block is $[[8, 3, 2]]_2$, the fixed gauge- X operators $G_{4,5,6}^X$ of the control are copied to the target under transversal CNOT, so the target block is taken out of the $[[8, 3, 2]]_2$ codespace. In the reverse direction, with $[[8, 3, 2]]_2$ as control and $[[8, 3, 2]]_1$ as target, no such fixed gauge- X operators are copied, so the codespace is preserved. Therefore a parallel inter-block logical $\overline{\text{CNOT}}$ is available between mixed-version blocks only in the direction $[[8, 3, 2]]_2 \rightarrow [[8, 3, 2]]_1$.

The logical circuit for a single-pair inter-block $\overline{\text{CNOT}}$ is shown in Fig. 3 [27]. It uses only logical SWAP gates, parallel inter-block logical $\overline{\text{CNOT}}$ gates, and in-block logical $\overline{\text{CNOT}}$ gates. Consequently, such a single-pair inter-block logical $\overline{\text{CNOT}}$ is available whenever those three ingredients are available. They are always available between two Version 1 blocks or between two Version 2 blocks in principle, but in practice, the Version 2 realization uses much simpler circuits to implement the intra-block logical $\overline{\text{CNOT}}$ gates. Between mixed-version blocks, the same asymmetry as above remains, so a single-pair inter-block logical $\overline{\text{CNOT}}$ is possible from $[[8, 3, 2]]_2$ to $[[8, 3, 2]]_1$ but not in the reverse direction.

An inter-block logical $\overline{\text{CCZ}}$ gate (with participating logical qubits initially residing in different blocks) can be implemented after first switching the relevant blocks into a compatible version (typically Version 2). One then uses inter-block logical SWAP operations implemented with inter-block $\overline{\text{CNOT}}$ gates to bring the three participating logical qubits into a common block, applies the in-block logical $\overline{\text{CCZ}}$ gate there, and finally reverses the

SWAPs to return the logical qubits back to their original blocks.

IV. CODE-SWITCHING BETWEEN TWO VERSIONS OF THE $[[8, 3, 2]]$ CODE

The two versions of the $[[8, 3, 2]]$ code differ in the states of the gauge qubits. Potentially, one could apply the logical \overline{H}_4 , \overline{H}_5 , and \overline{H}_6 to switch between the two versions. However, no fault-tolerant implementation of these gates has been found, as the logical \overline{X} and \overline{Z} operators have different weights in the two codes. Instead, we can measure the gauge operators to force the gauge qubits to be eigenstates of the logical \overline{X} or \overline{Z} operators, and apply unitary corrections if necessary. Next, we give a detailed description of the code-switching procedure.

A. Switching from Version 2 to 1

We measure the gauge X operators. Consider the example of a single physical qubit to clarify our understanding of gauge fixing. The single-qubit measurement of a $|0\rangle$ state in the X basis can yield either $+1$ when the measurement projects the state onto the $|+\rangle$ state, or -1 when the measurement projects the state onto the $|-\rangle$ state. If the measurement result is -1 , we can then apply a Z gate to change the state to $|+\rangle$. Measuring the gauge X operators similarly projects the gauge qubits onto the ± 1 eigenstate of the gauge X operators. If -1 results in any of the measurements, we apply the corresponding gauge Z operator to change it to $+1$. For example, if the result of measuring the three gauge X operators is $(-1, +1, +1)$, then we would apply $G_4^Z = Z_0 Z_1 Z_2 Z_3$. We call this the *gauge correction* to distinguish it from the correction in an error-correction code.

Next, we consider physical errors. Note that

$$G_4^X \cdot G_5^X \cdot G_6^X \cdot X_0 X_1 X_2 X_4 = X^{\otimes 8}. \quad (20)$$

Call $X_0 X_1 X_2 X_4$ the *complementary X check*, because the product of the measurements of G_4^X , G_5^X , G_6^X and $X_0 X_1 X_2 X_4$ is equivalent to measuring the $X^{\otimes 8}$ stabilizer. If the product is -1 , then there is a Z error, and we can discard the run before applying the gauge correction. Otherwise, we apply the gauge correction and continue the run. Measuring the complementary X check itself is not required merely to define the gauge correction itself, but it is required if the switched state will subsequently be used for logical computation. In that setting, the complementary check provides a low-weight surrogate for the $X^{\otimes 8}$ stabilizer and helps verify that the target code has been reached in the correct stabilizer sector before further logical gates are applied.

B. Switching from Version 1 to 2.

Similarly, we measure the gauge G^Z operators to switch from Version 1 to Version 2 and apply the corresponding G^X operation. To detect an X error, we can measure the complementary Z checks. For example, the complement of $G_4^Z = Z_0Z_1Z_2Z_3$ is

$$Z_4Z_5Z_6Z_7 = Z^{\otimes 8} \cdot Z_0Z_1Z_2Z_3. \quad (21)$$

Therefore, the product of the measurement results of G_4^Z and $Z_4Z_5Z_6Z_7$ is sufficient to detect any weight-1 X error.

C. Remarks on fault tolerance

A subtle but important point is that fault-tolerant code switching must do more than preserve detectability of weight-1 data errors. It must also ensure that, after switching, the state lies in the correct stabilizer sector of the target code before any subsequent logical gate is applied.

If a gauge measurement is faulty and its sign is left unchecked, the state may still be rejected by a later full stabilizer round, but the intended logical action in the target code can already be wrong. In the $[[8, 3, 2]]_2$ code, the transversal T/T^\dagger pattern implements the logical \overline{CCZ} gate only on the $+1$ eigenspace of the Z -type stabilizers, including G_4^Z , G_5^Z , and G_6^Z . Likewise, in the $[[8, 3, 2]]_1$ code, the essential weight-2 representations of the logical \overline{X} operators differ from their original weight-4 representations by products of G_4^X , G_5^X , and G_6^X . If one of these gauge operators has an eigenvalue of -1 because of the projection from measuring the gauge operators, then subsequent logical gates expressed in terms of the weight-2 representatives act with the wrong sign.

Our fault-tolerant code-switching protocol must prevent incorrectly applying the gauge operators, which causes logical errors, due to a single Pauli error. Meanwhile, leaving a single Pauli error undetected at the end of a subroutine is fault-tolerant as long as no other errors happen before the next error detection round. To achieve this, our protocol uses both the complementary check and the stabilizer verification.

When switching from Version 1 to Version 2, we measure the three gauge operators G_4^Z , G_5^Z , and G_6^Z , and we also measure the complementary check $Z_4Z_5Z_6Z_7$, so that the product of the outcomes of G_4^Z and $Z_4Z_5Z_6Z_7$ gives the $Z^{\otimes 8}$ syndrome before the gauge corrections are applied. With the complementary check, any single Pauli X or Y error before the gauge-fixing protocol or at the measurement ancilla can be detected (the Pauli Z errors are harmless now because they commute with the entire protocol), and the run will be discarded before any gauge operator is incorrectly applied. For example, assume the gauge G^Z measurement results should be $(+1, +1, +1)$ in the noiseless situation, where no gauge correction is

required. An X_3 error or an X error in the measurement ancilla of the gauge G_4^Z operator measurement will yield the measurement results $(-1, +1, +1)$, which incorrectly applies the gauge G_4^X operator. Although the complementary check detects any single Pauli X or Y error that occurs before the gauge-fixing protocol or on the measurement ancilla, it does not detect X or Y errors that occur between successive gauge measurements during the code-switching protocol.

Consider an X_0 error that happens after the gauge G_4^Z measurement. The measurement results become $(+1, -1, -1)$, and the complementary check $Z_4Z_5Z_6Z_7$ is also $+1$ because the X_0 error evades it. These measurement outcomes do not call for discard, so one will incorrectly apply the gauge G_5^X and G_6^X correction. To detect errors that happen during the code-switching protocol, we measure the final $Z^{\otimes 8}$ stabilizer after switching, because faults that occur between the gauge measurements may not be detected by the pre-correction complementary check alone. This protocol is summarized in Algorithm 1. Note that in Algorithm 1 (and also 2 below), $\text{Meas}(P)$ returns the eigenvalue ± 1 of the measured Pauli operator P .

Algorithm 1: Fault-tolerant code-switching protocol from Version 1 to Version 2

```

Measure the gauge  $G^Z$  operators  $M_4^Z \leftarrow \text{Meas}(G_4^Z)$ ,
 $M_5^Z \leftarrow \text{Meas}(G_5^Z)$ ,  $M_6^Z \leftarrow \text{Meas}(G_6^Z)$ ;
Measure the complementary operator
 $M_7^Z \leftarrow \text{Meas}(Z_4Z_5Z_6Z_7)$ ;
Measure the  $Z^{\otimes 8}$  stabilizer  $M_8^Z \leftarrow \text{Meas}(Z^{\otimes 8})$ ;
if  $\prod_{i=4,5,6,7} M_i^Z = +1$  and  $M_8^Z = +1$  then
  foreach  $i \in \{4, 5, 6\}$  such that  $M_i^Z = -1$  do
     $\lfloor$  Apply  $G_i^X$ 
  else
     $\lfloor$  Discard current run;

```

By symmetry, when switching from Version 2 to Version 1, we measure the three gauge operators G_4^X , G_5^X , and G_6^X , together with the complementary check $X_0X_1X_2X_3$, whose product with the three gauge outcomes is equivalent to measuring the $X^{\otimes 8}$ stabilizer. We also measure the final $X^{\otimes 8}$ stabilizer after switching. In this way, the target code is guaranteed to be in the correct gauge and stabilizer sector before the Version 1 logical gates are applied. This protocol is summarized in Algorithm 2.

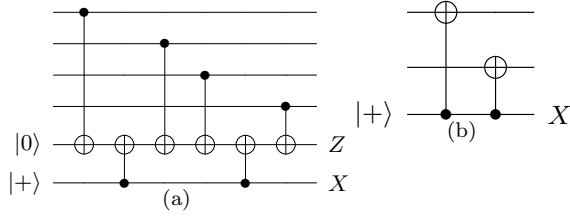


FIG. 4. (a) Flag-based measurement of a weight-4 Z -type gauge operator used in switching from Version 1 to Version 2. The upper four wires are the data qubits in the support of the measured operator, the fifth wire is the ancilla measured in the Z basis to decide whether G^X corrections are necessary, and the last wire is a flag ancilla measured in the X basis. A triggered flag identifies single-fault events that can propagate to weight-2 Z errors on the data qubits. (b) Fault-tolerant measurement of a weight-2 X -type gauge operator used in switching from Version 2 to Version 1. The upper two wires are the data qubits in the support of the measured operator, the third wire is the ancilla measured in the X basis to decide whether G^Z corrections are necessary. Because the measured operator has weight 2, no flag ancilla is required.

Algorithm 2: Fault-tolerant code-switching protocol from Version 2 to Version 1

Measure the gauge G^X operators
 $M_4^X \leftarrow \text{Meas}(G_4^X), M_5^X \leftarrow \text{Meas}(G_5^X),$
 $M_6^X \leftarrow \text{Meas}(G_6^X);$
 Measure the complementary operator
 $M_7^X \leftarrow \text{Meas}(X_0 X_1 X_2 X_4);$
 Measure the $X^{\otimes 8}$ stabilizer $M_8^X \leftarrow \text{Meas}(X^{\otimes 8});$
if $\prod_{i=4,5,6,7} M_i^X = +1$ **and** $M_8^X = +1$ **then**
 | **foreach** $i \in \{4, 5, 6\}$ **such that** $M_i^X = -1$ **do**
 | | Apply G_i^Z
else
 | Discard current run;

Like syndrome extraction, our gauge operator measurement requires flag qubits [31] to detect a weight-1 error on the ancilla, which propagates to higher-weight errors on the data qubits. When we switch from Version 1 to Version 2, the flag qubits are required as the measured G^Z gauge operators are weight-4, where a weight-1 Z error on the ancilla can propagate to a weight-2 error on the data qubits. Meanwhile, switching from Version 2 to Version 1 does not require flag qubits, because the measured G^X gauge operators are weight-2 and do not propagate a higher-weight error.

V. FAULT-TOLERANT ENCODING CIRCUITS

In this section, we construct fault-tolerant state-preparation circuits for both versions of the $[[8, 3, 2]]$ code. The states $|000\rangle$ and $|++++\rangle$ can be prepared fault-tolerantly in both versions. We also consider mixed logical-basis states. Without any additional gauge fix-

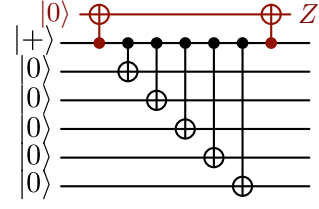


FIG. 5. Fault-tolerant GHZ state encoding circuit [31]. The black part is the encoding circuit, and the red part checks for error propagation.

ing, we prepare $|+^2 0^1\rangle$ in the Version 1 code and $|+^1 0^2\rangle$ in the Version 2 code. For applications that require the opposite pairing, namely $|+^2 0^1\rangle$ in Version 2 or $|+^1 0^2\rangle$ in Version 1, we prepare a partially gauge-fixed intermediate state and then perform only the single remaining gauge-fixing step rather than a full code switch.

Here the notation $|+^j 0^{n-2-j}\rangle$ specifies only the number of $|+\rangle$ and $|0\rangle$ logical states, not their ordering. The simulation results for all of the state-preparation circuits described below are shown in Fig. 14 and Fig. 15.

A. The GHZ state

This section extensively utilizes the GHZ state and the dual GHZ state. We provide their definitions and fault-tolerant encoding circuits here. An n -qubit Greenberger-Horne-Zeilinger (GHZ) state [32] written in the computational (Z) basis is

$$|\text{GHZ}_n\rangle = \frac{1}{\sqrt{2}} (|0\rangle^{\otimes n} + |1\rangle^{\otimes n}). \quad (22)$$

Its $+1$ eigenoperators are $X^{\otimes n}$ and $Z_0 Z_j$ for $j = 1, \dots, n-1$. A dual GHZ state written in the X basis is

$$|\text{Dual GHZ}_n\rangle = \frac{1}{\sqrt{2}} (|+\rangle^{\otimes n} + |-\rangle^{\otimes n}). \quad (23)$$

Its $+1$ eigenoperators are $Z^{\otimes n}$ and $X_0 X_j$ for $j = 1, \dots, n-1$.

The fault-tolerant encoding circuit of the GHZ state is shown in Fig. 5. The fault-tolerant encoding circuit for the dual GHZ state is the same as the circuit in the X basis. (That is, we replace $|0\rangle$ with $|+\rangle$, replace $|+\rangle$ with $|0\rangle$, invert all CNOT gates, and change the measurement from the Z to the X basis.)

B. Encoding logical $|000\rangle$ and $|++++\rangle$ states

a. Logical $|000\rangle$ state for the Version 2 $[[8, 3, 2]]$ code (Fig. 13(a)). This is equivalent to fixing all three logical qubits and all three gauge qubits of the $[[8, 3, 3, 2]]$

subsystem code to $|\bar{0}\rangle$ and $|0_g\rangle$, respectively. The +1-eigenoperators can be reduced with Gaussian elimination:

$$\begin{aligned}
\bar{Z}_1 &= Z_0 Z_4 \rightarrow Z_0 Z_4 \\
\bar{Z}_2 &= Z_0 Z_2 \rightarrow Z_0 Z_2 \\
\bar{Z}_3 &= Z_0 Z_1 \rightarrow Z_0 Z_1 \\
G_4^Z &= Z_0 Z_1 Z_2 Z_3 \rightarrow Z_0 Z_3 \\
G_5^Z &= Z_0 Z_1 Z_4 Z_5 \rightarrow Z_0 Z_5 \\
G_6^Z &= Z_0 Z_2 Z_4 Z_6 \rightarrow Z_0 Z_6 \\
S^X &= X^{\otimes 8} \rightarrow X^{\otimes 8} \\
S^Z &= Z^{\otimes 8} \rightarrow Z_0 Z_7
\end{aligned} \tag{24}$$

This is the 8-qubit GHZ state and can be prepared in the same fault-tolerant way.

b. Logical $|\overline{+++}\rangle$ state for the Version 1 $[[8,3,2]]$ code (Fig. 12(d)). Similarly, this is equivalent to fixing all three logical qubits and all three gauge qubits of the $[[8,3,3,2]]$ subsystem code to $|\bar{\mp}\rangle$ and $|+_g\rangle$, respectively. The +1-eigenoperators can be reduced with Gaussian elimination:

$$\begin{aligned}
\bar{X}_1 &= X_0 X_1 X_2 X_3 \rightarrow X_6 X_4 \\
\bar{X}_2 &= X_0 X_1 X_4 X_5 \rightarrow X_6 X_2 \\
\bar{X}_3 &= X_0 X_2 X_4 X_6 \rightarrow X_6 X_1 \\
G_4^X &= X_7 X_3 \rightarrow X_3 X_6 \\
G_5^X &= X_7 X_5 \rightarrow X_5 X_6 \\
G_6^X &= X_7 X_6 \rightarrow X_7 X_6 \\
S^X &= X^{\otimes 8} \rightarrow X_0 X_6 \\
S^Z &= Z^{\otimes 8} \rightarrow Z^{\otimes 8}
\end{aligned} \tag{25}$$

This is the 8-qubit dual GHZ state and can be prepared in the same fault-tolerant way.

c. Logical $|000\rangle$ state for the Version 1 $[[8,3,2]]$ code (Fig. 12(a)). This preparation fixes all three logical qubits and all three gauge qubits of the $[[8,3,3,2]]$ subsystem code to $|\bar{0}\rangle$ and $|+_g\rangle$, respectively. Since all logical and gauge operators are weight-2, we can borrow the fault-tolerant encoding circuit that prepares the logical state $|\overline{+^j 0^{n-j-2}}\rangle$ in the $[[n, n-2, 2]]$ code from [31], despite a different choice of basis. In particular, the state preparation we need is equivalent to preparing the logical $|\overline{+^3 0^3}\rangle$ state in the $[[8,6,2]]$ stabilizer code with the logical operator basis

$$X_k X_7, \quad Z_0 Z_k, \quad k = 1, \dots, 6. \tag{26}$$

Here, since $j = 3$ is odd, the logical state $|\overline{+^3 0^3}\rangle$ is the product of a GHZ state and a dual GHZ state. Explicitly, it is

$$\begin{aligned}
|\overline{+^3 0^3}\rangle &= \frac{1}{\sqrt{2}}(|_{+3 +5 +6 +7}\rangle + |_{-3 -5 -6 -7}\rangle) \\
&\otimes \frac{1}{\sqrt{2}}(|_{0_0 0_1 0_2 0_4}\rangle + |_{1_0 1_1 1_2 1_4}\rangle).
\end{aligned} \tag{27}$$

Given the fault-tolerant circuits to prepare the four-qubit GHZ and dual GHZ state, we can prepare the logical $|\overline{+^3 0^3}\rangle$ state of the $[[8,6,2]]$ stabilizer code, which is equivalent to the logical $|000\rangle$ state for the Version 1 $[[8,3,2]]$ code.

d. Logical $|\overline{+++}\rangle$ state for the Version 2 $[[8,3,2]]$ code (Fig. 13(d)). A circuit for this has already been proposed in [29].

C. Encoding logical $|\overline{+^2 0^1}\rangle$ and $|\overline{+^1 0^2}\rangle$ states without gauge-fixing

a. Logical $|\overline{+^2 0^1}\rangle$ state for the Version 1 $[[8,3,2]]$ code (Fig. 12(c)). The logical state $|\overline{+^2 0^1}\rangle$ is a product of a GHZ state and a dual GHZ state. For example, the logical $|\overline{++0}\rangle$ state has +1 eigenoperators that can be reduced with Gaussian elimination which is identical to the logical $|\overline{+++}\rangle$ state except for $X^{\otimes 8} \rightarrow X_0 X_1$. With the additional $Z_0 Z_1$ operator, we have a GHZ state (Bell state) on qubits 0 and 1 and a dual GHZ state on the rest of the qubits.

$$\begin{aligned}
&|\overline{++0}\rangle \\
&= \frac{1}{\sqrt{2}}(|_{+3 +5 +6 +7 +2 +4}\rangle + |_{-3 -5 -6 -7 -2 -4}\rangle) \\
&\otimes \frac{1}{\sqrt{2}}(|_{0_0 0_1}\rangle + |_{1_0 1_1}\rangle).
\end{aligned} \tag{28}$$

The preparation circuit of the Bell state is fault-tolerant without ancillas, and the 6-qubit dual GHZ state can be prepared in a fault-tolerant method with one ancilla. Other orderings of $|\overline{+^2 0^1}\rangle$ can be prepared similarly.

b. Logical $|\overline{+^1 0^2}\rangle$ state for the Version 2 $[[8,3,2]]$ code (Fig. 13(b)). We use the logical $|\overline{00+}\rangle$ state as an example. We list below all the +1-eigenoperators when the initial state is prepared, along with their reduced forms via Gaussian elimination.

$$\begin{aligned}
\bar{Z}_1 &= Z_0 Z_4 \rightarrow Z_0 Z_4 \\
\bar{Z}_2 &= Z_0 Z_2 \rightarrow Z_0 Z_2 \\
\bar{X}_3 &= X_0 X_2 X_4 X_6 \rightarrow X_0 X_2 X_4 X_6 \\
G_4^Z &= Z_0 Z_1 Z_2 Z_3 \rightarrow Z_1 Z_3 \\
G_5^Z &= Z_0 Z_1 Z_4 Z_5 \rightarrow Z_1 Z_5 \\
G_6^Z &= Z_0 Z_2 Z_4 Z_6 \rightarrow Z_0 Z_6 \\
S^X &= X^{\otimes 8} \rightarrow X_1 X_3 X_5 X_7 \\
S^Z &= Z^{\otimes 8} \rightarrow Z_1 Z_7
\end{aligned} \tag{29}$$

These reduced generators describe two independent four-qubit GHZ states: one on the even qubits $\{0, 2, 4, 6\}$ and one on the odd qubits $\{1, 3, 5, 7\}$. Hence, the state can be prepared by fault-tolerantly preparing these two GHZ states.

D. Encoding logical $|\overline{+20^1}\rangle$ and $|\overline{+10^2}\rangle$ states with gauge fixing

a. *Logical $|\overline{+20^1}\rangle$ state for the Version 2 $[[8, 3, 2]]$ code (Fig. 13(c)).* We use the logical $|\overline{++0}\rangle$ state as an example. We first need to fix the gauge operators G_4^Z , G_5^Z , and G_6^X . We list below all the $+1$ -eigenoperators when the initial state is prepared and what they become in a reduced form via Gaussian elimination:

$$\begin{aligned}
\overline{X}_1 &= X_0X_1X_2X_3 \rightarrow X_4X_5 \\
\overline{X}_2 &= X_0X_1X_4X_5 \rightarrow X_0X_1 \\
\overline{Z}_3 &= Z_0Z_1 \rightarrow Z_0Z_1 \\
G_4^Z &= Z_0Z_1Z_2Z_3 \rightarrow Z_2Z_3 \\
G_5^Z &= Z_0Z_1Z_4Z_5 \rightarrow Z_4Z_5 \\
G_6^X &= X_7X_6 \rightarrow X_7X_6 \\
S^X &= X^{\otimes 8} \rightarrow X_2X_3 \\
S^Z &= Z^{\otimes 8} \rightarrow Z_7Z_6
\end{aligned} \tag{30}$$

These operators constitute four Bell states on four pairs of qubits: $\{0, 1\}$, $\{2, 3\}$, $\{4, 5\}$, and $\{6, 7\}$, which are fault-tolerant without any ancilla. After the logical state is prepared, we perform the remaining gauge-fixing step by measuring $G_6^Z = Z_0Z_2Z_4Z_6$. At the same stage, we measure its complementary check $Z_1Z_3Z_5Z_7$, whose product with G_6^Z gives the $Z^{\otimes 8}$ syndrome and detects faults that would leave the switched state in the wrong stabilizer sector for subsequent logical operations. Here we do not include an additional dedicated $Z^{\otimes 8}$ stabilizer measurement inside this final gauge-fixing subroutine. Unlike the full code-switching protocol, only one gauge operator remains to be measured, so there are no later gauge measurements whose outcomes can be corrupted by an intermediate fault. The complementary check is therefore sufficient to prevent an incorrect application of the gauge correction. Any residual data error, such as an error occurring after the gauge measurement, is handled by the full stabilizer round applied immediately after state preparation.

b. *Logical $|\overline{+10^2}\rangle$ state for the Version 1 $[[8, 3, 2]]$ code (Fig. 12(b)).* We use the logical $|\overline{00+}\rangle$ state as an example. We first fix the gauge operators G_4^X , G_5^X , and G_6^Z . We list below all the $+1$ -eigenoperators when the initial state is prepared, along with their reduced forms via Gaussian elimination:

$$\begin{aligned}
\overline{Z}_1 &= Z_0Z_4 \rightarrow Z_0Z_4 \\
\overline{Z}_2 &= Z_0Z_2 \rightarrow Z_0Z_2 \\
\overline{X}_3 &= X_0X_2X_4X_6 \rightarrow X_1X_7 \\
G_4^X &= X_7X_3 \rightarrow X_7X_3 \\
G_5^X &= X_7X_5 \rightarrow X_7X_5 \\
G_6^Z &= Z_0Z_2Z_4Z_6 \rightarrow Z_0Z_6 \\
S^X &= X^{\otimes 8} \rightarrow X_0X_2X_4X_6 \\
S^Z &= Z^{\otimes 8} \rightarrow Z_1Z_3Z_5Z_7
\end{aligned} \tag{31}$$

Observe that the reduced operators form a 4-qubit GHZ state on qubits $\{0, 2, 4, 6\}$ and a 4-qubit dual GHZ state on qubits $\{1, 3, 5, 7\}$. Hence, the ability to prepare the GHZ state and the dual GHZ state fault-tolerantly is sufficient. After the logical state is prepared, we perform the remaining gauge-fixing step by measuring $G_6^X = X_7X_6$. At the same stage, we measure its complementary check $X_0X_1X_2X_3X_4X_5$, whose product with G_6^X gives the $X^{\otimes 8}$ syndrome before the correction is applied. Here we do not include an additional dedicated $X^{\otimes 8}$ stabilizer measurement inside this final gauge-fixing subroutine. Unlike the full code-switching protocol, only one gauge operator remains to be measured, so there are no later gauge measurements whose outcomes can be corrupted by an intermediate fault. The complementary check is therefore sufficient to prevent an incorrect application of the gauge correction. Any residual data error, such as an error occurring after the gauge measurement, is handled by the full stabilizer round applied immediately after state preparation.

VI. SIMULATION

In this section, we use numerical simulations to evaluate the logical error rates of our state-preparation circuits and code-switching protocol in the presence of faulty gates. A faulty gate is modeled as $\tilde{\mathcal{U}} = \mathcal{N} \circ \mathcal{U}$, where $\mathcal{U}(\rho) = U\rho U^\dagger$ is a noise-free unitary channel and \mathcal{N} is the noise channel associated with the gate. In our simulations, we adopt the depolarizing noise channel for all two-qubit gates with physical error rate p and for all single-qubit gates with physical error rate q . For simplicity, we neglect noise from physical qubit initialization, measurements, feedback, and corrections. The single-qubit and two-qubit depolarizing channels are given by

$$\mathcal{N}_1(\rho) = (1 - q)\rho + \frac{q}{3} \sum_j P_j \rho P_j, \tag{32}$$

$$\mathcal{N}_2(\rho) = (1 - p)\rho + \frac{p}{15} \sum_j P_j \rho P_j. \tag{33}$$

where $\{P_j\}$ are all possible single/two-qubit Pauli operators except the identity. Thus, one of the possible single-qubit Pauli errors is applied with probability $q/3$ after each single-qubit gate, and one of the possible two-qubit Pauli errors is applied with probability $p/15$ after each two-qubit gate. All numerical simulations in this section are performed using the Python package PECOS, a tool designed for efficient Monte-Carlo simulations of quantum Clifford circuits, and we assume $q = p/10$ for single-qubit error rates.

A. State preparation

The outcome of state preparation in the presence of noise falls into three categories: successful preparation,

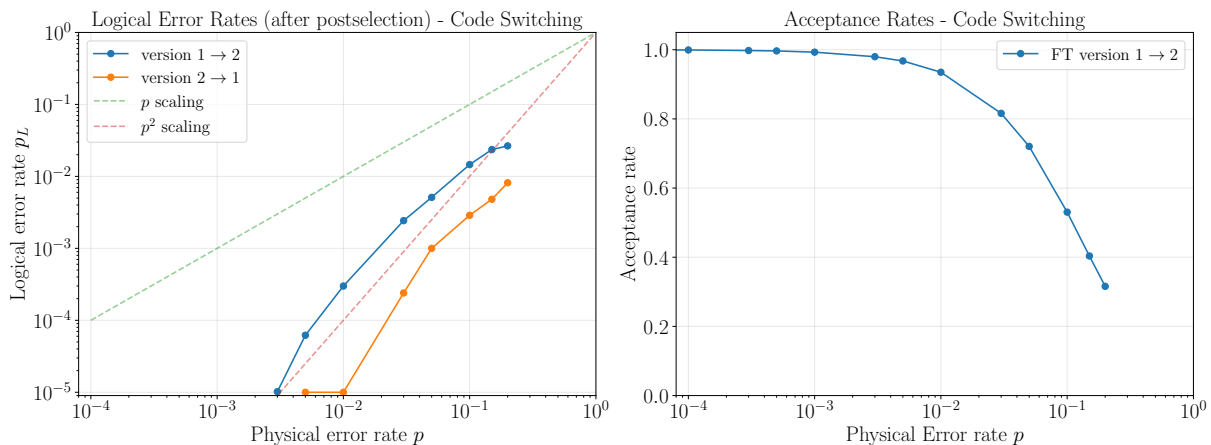


FIG. 6. Logical error rates and acceptance rates of code-switching obtained from numerical simulation. Here, we consider depolarizing noise with physical error rate p for all CNOT gates and $q = p/10$ for all single-qubit gates in our simulation. For simplicity, we assume the feedback and correction process is noise-free. For switching from Version 1 to 2, we use the flagged circuits in Fig. 4 for weight-4 Pauli-Z measurements. The weight-2 Pauli-X measurements for switching from Version 2 to 1 are fault-tolerant without any flag qubits.

discarded runs, and failed preparation. A preparation is successful if the resulting state matches the desired state up to stabilizers. When the circuit produces erroneous states, some can be detected by measuring the flag qubits and subsequently discarded via postselection, while others remain undetected and result in a failed preparation with logical errors. In our numerical simulations, we identify failed preparations based on measurements of stabilizers and logical operators. For example, preparing the logical $|++\rangle$ state for Version 1 of the $[[8, 3, 2]]$ code counts as a failure if the output state is a $+1$ eigenstate of the stabilizers in Eq. (10) but not a $+1$ eigenstate of the logical operators \bar{X}_1, \bar{X}_2 , and \bar{X}_3 defined in Eq. (11).

Fig. 14 and Fig. 15 show the logical error rate and acceptance rate for state preparation circuits in Versions 1 and 2 of the $[[8, 3, 2]]$ code after 100,000 simulations, respectively. We define the logical error rate as

$$p_L = \frac{n_{\text{failure}}}{n_{\text{postselected}}}, \quad (34)$$

and the acceptance rate as a fraction of postselected runs among total runs,

$$R = \frac{n_{\text{postselected}}}{n_{\text{total}}}. \quad (35)$$

Note that since both versions of the $[[8, 3, 2]]$ code can only detect but not correct errors, the logical error rate should reflect the fidelity of the state after error detection and postselection. In the regime of physical error rate $p < 0.1$, the logical error rate p_L scales quadratically with the physical error rate p , indicating that the state preparation circuits proposed in Section V are indeed fault-tolerant and only weight-2 (or above) errors contribute to p_L in these circuits.

B. Code switching

In this subsection, we simulate the code-switching protocol between the two versions of the $[[8, 3, 2]]$ code described in Section IV, which involves measuring extra stabilizers and applying Pauli corrections based on the measurement outcome. In the presence of noise, there are three possible outcomes: successful code switching, a discarded run, and failed code switching. The switching protocol is considered successful if the logical information is preserved during the process. If any stabilizer measurements return -1 , a detectable error has occurred, and the current shot should be discarded. If all measurements return $+1$ but the logical state has been changed, the run still contains a logical error and should be treated as a failure.

To evaluate the performance of the code-switching protocol, we prepare a logical $|++\rangle$ state in Version 1 and count the number of failures in code switching under different physical error rates. Since the focus of simulation in this subsection is purely on the code switching itself, we use the circuits in Fig. 12 with noise-free gates to construct a noise-free $|++\rangle$ state. Flag qubits are used for fault-tolerant measurement of three weight-4 Pauli-Z operators for code-switching (see Fig. 4 or Ref.[31] for details), which prevents any weight-1 error in the ancilla qubit from propagating to a logical error in the data qubits. The gauge corrections are applied only when all flag qubits are measured to be $+1$. In the code-switching from Version 2 to Version 1, the measurement of three weight-2 Pauli-X operators does not require flag qubits, because an error in the ancilla either propagates to a weight-1 error or a weight-2 stabilizer.

Fig. 6 shows the results of the fault-tolerant code-switching protocol obtained from 100,000 shots of nu-

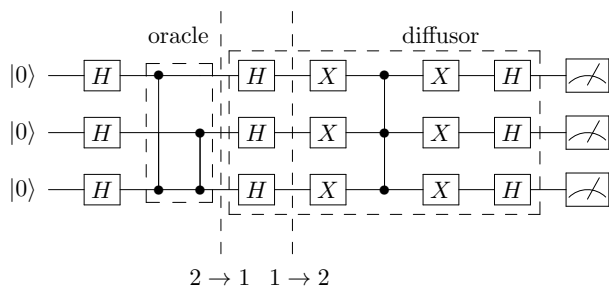


FIG. 7. Logical circuit for Grover’s search algorithm that finds two solutions $x_0 = 011$ or $x_0 = 101$ out of 8 candidates. The vertical dashed lines show the positions of the code switchings.

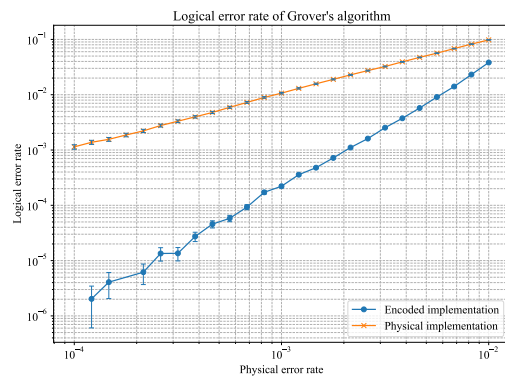
merical simulation and demonstrates quadratic scaling $p_L \sim p^2$ for fault-tolerant code-switching in both directions. Here, a resulting state is counted as a failure if it is a +1 eigenstate of the stabilizers but not a +1 eigenstate of the logical operators \bar{X}_1, \bar{X}_2 , and \bar{X}_3 . The run is discarded if the resulting state is not a +1 eigenstate of the stabilizers, or if the flag qubit is triggered during the measurement of the weight-4 Pauli operators. Given the number of failures and number of runs after postselection, we calculate the logical error rates and acceptance rates using Eqs. (34) and (35), and plot them in Fig. 6. Both simulations isolate the switching step itself and postselect immediately on the target-code stabilizers. Therefore, their quadratic scaling shows that, under this diagnostic, the switching step preserves the logical state in the error-detecting sense. For subsequent logical computation, however, we still include the complementary checks discussed in Section IV to ensure that the target code is reached in the correct gauge and stabilizer sector.

VII. GROVER’S ALGORITHM WITH CODE-SWITCHING

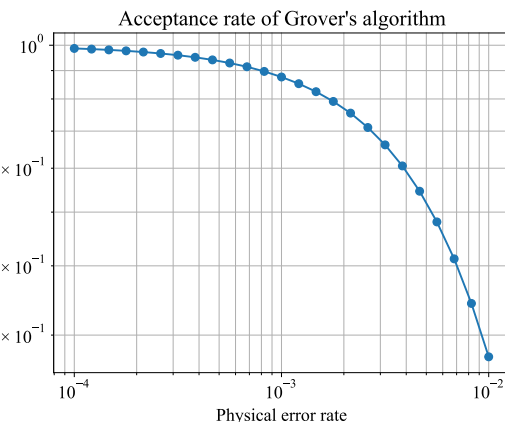
We demonstrate our ability to perform fault-tolerant universal computation with Grover’s algorithm. Grover’s algorithm is designed to search for a set of target (“marked”) binary strings $M \subseteq \{0,1\}^n$ in an unstructured database of size $N = 2^n$, where the oracle operator O is defined as

$$O|x\rangle = \begin{cases} -|x\rangle & x \in M \\ |x\rangle & \text{Otherwise} \end{cases} \quad (36)$$

for any n -bit binary string x . A classical algorithm requires $O(N/|M|)$ oracle calls, while the Grover algorithm has a quadratic speedup that requires $O(\sqrt{N}/|M|)$ oracle calls [33]. Fig. 7 shows an example of Grover’s algorithm that searches for solutions $M = \{101, 011\}$ from 8 possible candidates. In the ideal noiseless circuit, one Grover iteration maps the initial state entirely into the span of



(a)



(b)

FIG. 8. Simulation results for Grover’s algorithm. Panel (a) shows the output failure probability for the unencoded (physical) three-qubit circuit and the postselected logical failure probability for the encoded code-switching implementation. The unencoded circuit exhibits linear scaling with the physical error rate, whereas the encoded implementation exhibits quadratic scaling in the low-noise regime. Panel (b) shows the acceptance rate of the postselected encoded implementation.

$|101\rangle$ and $|011\rangle$, and no other output bit string occurs. As a result, all other outputs in noisy circuits are considered logical errors. The Grover algorithm is a good small-scale demonstration of our protocol because its oracle requires both the H gate and the CCZ gate, which is impossible without code-switching between two versions of the $[[8, 3, 2]]$ code for fault-tolerant implementations.

To evaluate the performance of Grover’s algorithm with code switching, we simulated both the unencoded three-qubit circuit and the encoded code-switching implementation using `Qiskit Aer Simulator`. For each physical error rate between 10^{-4} and 10^{-2} , we sampled 10^6 shots. In the encoded simulation, postselection is applied on all stabilizer and flag measurements associated with state preparation and code switching, and a postselected shot is counted as successful if the eight data qubits de-

code to either of the Version 2 logical states $|\overline{101}\rangle$ or $|\overline{011}\rangle$. In the unencoded simulation, a shot is counted as successful if the measured three-bit output is 101 or 011.

We define the failure probability in each case as the fraction of shots that do not yield one of the marked outputs among all the accepted runs. The results are shown in Fig. 8. The unencoded circuit exhibits linear scaling of the output failure probability with the physical error rate, while the encoded code-switching implementation exhibits quadratic scaling of the postselected logical failure probability in the low-noise regime.

VIII. CONCLUSION

In this paper, we developed a fault-tolerant, error-detecting protocol for switching between two versions of the $[[8, 3, 2]]$ code and used it to assemble a universal logical gate set. Numerical simulations of state preparation, code switching, and a three-logical-qubit Grover search show quadratic suppression of postselected logical error rates, consistent with weak fault tolerance.

We showed that both versions arise from the same $[[8, 3, 3, 2]]$ subsystem code, obtained by gauging out three logical qubits of the $[[8, 6, 2]]$ code after a noncanonical choice of logical basis. Fixing the gauge qubits in $|0_g\rangle$ yields Version 2, namely the $[[8, 3, 2]]$ code with logical \overline{CCZ} , \overline{CZ} , \overline{CNOT} , and \overline{SWAP} gates. Fixing them in $|+_g\rangle$ yields Version 1, in which the resulting weight-2 representatives of the logical operators enable weakly fault-tolerant implementations of \overline{H} , \overline{S} , and $\overline{\sqrt{X}}$ using the \overline{XX} and \overline{ZZ} rotation gadgets. We also showed that single inter-block logical \overline{CNOT} gates are available between same-version blocks and, for mixed-version blocks, only in the direction $[[8, 3, 2]]_2 \rightarrow [[8, 3, 2]]_1$.

We also clarified the role of complementary checks in

distance-2 code switching. In our setting, they are not optional if the switched state is to be used for subsequent logical computation: together with the final stabilizer measurement, they ensure that the target code is reached in the correct gauge and stabilizer sector before further logical gates are applied. Operationally, they provide low-weight surrogates for directly measuring the weight-8 stabilizers and thereby reduce the overhead of stabilizer verification during switching.

Finally, our construction suggests a broader family viewpoint. The code $[[8, 3, 2]]_2$ belongs to the $[[2^D, D, 2]]$ hypercube family with $D = 3$, while the parent $[[8, 6, 2]]$ code belongs to the $[[n, n - 2, 2]]$ family. Our use of a noncanonical logical basis raises the question of how to choose logical bases systematically for $[[2^D, 2^D - 2, 2]]$ codes so that $2^D - 2 - D$ logical qubits may be gauged out while preserving useful transversal structure. Fixing those gauge qubits in $|0_g\rangle$ recovers the D -dimensional hypercube code, while fixing them in $|+_g\rangle$ suggests a companion family generalizing our Version 1 construction. More generally, D -dimensional hypercube codes support transversal controlled-phase gates of increasing order, providing depth-1 access to higher levels of the Clifford hierarchy. It would therefore be interesting to characterize the corresponding Version 1 family systematically and to determine its transversal logical gate set.

ACKNOWLEDGEMENTS

The authors acknowledge Christopher Gerhard, Anirudh Lanka and Juan Garcia Nila for useful discussions. This material is based upon work supported by, or in part by, the U. S. Army Research Laboratory and the U. S. Army Research Office under contract/grant number W911NF2310255 and by NSF Grant FET-2316713.

-
- [1] P. W. Shor, Scheme for reducing decoherence in quantum computer memory, *Phys. Rev. A* **52**, R2493 (1995).
 - [2] A. M. Steane, Error correcting codes in quantum theory, *Phys. Rev. Lett.* **77**, 793 (1996).
 - [3] D. Gottesman, *Stabilizer codes and quantum error correction*, Ph.D. thesis, California Institute of Technology, Pasadena, CA (1997).
 - [4] A. R. Calderbank, E. M. Rains, P. W. Shor, and N. J. A. Sloane, Quantum error correction and orthogonal geometry, *Physical Review Letters* **78**, 405 (1997).
 - [5] E. Knill and R. Laflamme, Theory of quantum error-correcting codes, *Phys. Rev. A* **55**, 900 (1997).
 - [6] F. Gaitan, *Quantum Error Correction and Fault Tolerant Quantum Computing* (Taylor & Francis Group, Boca Raton, 2008).
 - [7] D. Lidar and T. Brun, eds., *Quantum Error Correction* (Cambridge University Press, Cambridge, UK, 2013).
 - [8] D. Aharonov and M. Ben-Or, Fault-tolerant quantum computation with constant error, in *Proceedings of the twenty-ninth annual ACM symposium on Theory of computing* (1997) pp. 176–188.
 - [9] P. Aliferis, D. Gottesman, and J. Preskill, Quantum accuracy threshold for concatenated distance-3 codes, *Quant. Inf. Comput.* **6**, 97 (2006).
 - [10] B. W. Reichardt, Fault-tolerance threshold for a distance-three quantum code, in *Automata, Languages and Programming: 33rd International Colloquium, ICALP 2006, Venice, Italy, July 10-14, 2006, Proceedings, Part I*, edited by M. Bugliesi, B. Preneel, V. Sassone, and I. Wegener (Springer Berlin Heidelberg, Berlin, Heidelberg, 2006) pp. 50–61.
 - [11] E. Knill, Quantum computing with realistically noisy devices, *Nature* **434**, 39 (2005).
 - [12] E. T. Campbell, B. M. Terhal, and C. Vuillot, Roads towards fault-tolerant universal quantum computation, *Nature* **549**, 172 EP (2017).
 - [13] P. W. Shor, Fault-tolerant quantum computation, *Proceedings of 37th Conference on Foundations of Computer*

- Science*, **56** (1996).
- [14] B. Eastin and E. Knill, Restrictions on transversal encoded quantum gate sets, *Physical review letters* **102**, 110502 (2009).
- [15] C. Gerhard and T. A. Brun, Weakly fault-tolerant computation in a quantum error-detecting code (2024), [arXiv:2408.14828 \[quant-ph\]](https://arxiv.org/abs/2408.14828).
- [16] A. Y. Kitaev, Quantum computations: algorithms and error correction, *Russian Mathematical Surveys* **52**, 1191 (1997).
- [17] P. Boykin, T. Mor, M. Pulver, V. Roychowdhury, and F. Vatan, On universal and fault-tolerant quantum computing: a novel basis and a new constructive proof of universality for Shor's basis, in *40th Annual Symposium on Foundations of Computer Science* (IEEE Comput. Soc., Los Alamitos, CA, 1999) p. 486, [quant-ph/9906054](https://arxiv.org/abs/quant-ph/9906054).
- [18] S. Bravyi and A. Kitaev, Universal quantum computation with ideal clifford gates and noisy ancillas, *Physical Review A* **71**, 022316 (2005).
- [19] D. Litinski, Magic State Distillation: Not as Costly as You Think, *Quantum* **3**, 205 (2019).
- [20] J. T. Anderson, G. Duclos-Cianci, and D. Poulin, Fault-tolerant conversion between the steane and reed-muller quantum codes, *Physical Review Letters* **113**, 080501 (2014).
- [21] H. Bombín, Gauge color codes: optimal transversal gates and gauge fixing in topological stabilizer codes, *New Journal of Physics* **17**, 083002 (2015).
- [22] A. Kubica and M. E. Beverland, Universal transversal gates with color codes: A simplified approach, *Physical Review A* **91**, 032330 (2015).
- [23] D.-X. Quan, L.-L. Zhu, C.-X. Pei, and B. C. Sanders, Fault-tolerant conversion between adjacent reed-muller quantum codes based on gauge fixing, *Journal of Physics A: Mathematical and Theoretical* **51**, 115305 (2018).
- [24] F. Butt *et al.*, Fault-tolerant code-switching protocols for near-term quantum processors, *PRX Quantum* **5**, 020345 (2024).
- [25] M. Vasmer and A. Kubica, Morphing quantum codes, *PRX Quantum* **3**, 030319 (2022).
- [26] E. T. Campbell, [The smallest interesting colour code](https://arxiv.org/abs/1605.06068) (2016).
- [27] D. Hangleiter, M. Kalinowski, D. Bluvstein, M. Cain, N. Maskara, X. Gao, A. Kubica, M. D. Lukin, and M. J. Gullans, Fault-tolerant compiling of classically hard instantaneous quantum polynomial circuits on hypercubes, *PRX Quantum* **6**, 020338 (2025).
- [28] Y. Wang *et al.*, Fault-tolerant one-bit addition with the smallest interesting color code, *Science Advances* **10**, eado9024 (2024).
- [29] D. Honciuc Menendez, A. Ray, and M. Vasmer, Implementing fault-tolerant non-clifford gates using the $[[8,3,2]]$ color code, *Phys. Rev. A* **109**, 062438 (2024).
- [30] D. Bluvstein *et al.*, Logical quantum processor based on reconfigurable atom arrays, *Nature* **626**, 58 (2024).
- [31] R. Chao and B. W. Reichardt, Quantum error correction with only two extra qubits, *Physical review letters* **121**, 050502 (2018).
- [32] D. M. Greenberger, M. A. Horne, and A. Zeilinger, Going beyond bell's theorem, in *Bell's theorem, quantum theory and conceptions of the universe* (Springer, 1989) pp. 69–72.
- [33] L. K. Grover, A fast quantum mechanical algorithm for database search, in *Proceedings of the twenty-eighth annual ACM symposium on Theory of computing* (1996) pp. 212–219.

Appendix A: Fault-tolerant implementations of two-qubit rotation gates and Hadamard gate

Fig. 9 and Fig. 10 are the fault-tolerant implementations of the \widetilde{XX} and \widetilde{ZZ} gates taken from Ref. [15]. Both implementations have two versions. In the first version, ancillas are prepared in a Bell state and end in a $|++\rangle$ state, while in the second version ancillas are prepared in the $|++\rangle$ state and end in a Bell state. Hence, using two versions alternately avoids the need to re-prepare the ancillas. After each circuit, Pauli operations are applied according to Table II.

	\widetilde{ZZ} rotation	\widetilde{XX} rotation
$ \Phi_+\rangle$	$ZIZI$	$IZYI$
$ ++\rangle$	$XIXI$	$YIYI$

TABLE II. Pauli recovery operations to apply after each weakly fault-tolerant \widetilde{XX} or \widetilde{ZZ} gate. The row is determined by the state the ancilla qubits are indirectly in before the gate, and the column by which rotation gate we are implementing.

The logical Hadamard gate can be implemented by using the decomposition in Eq. (13). To avoid re-preparing the ancillas between successive two-qubit-rotation gadgets, one may choose the gadget versions so that the ancilla output of one gadget is the required ancilla input of the next: use a Bell-to- $|++\rangle$ version of \widetilde{ZZ} , followed by a $|++\rangle$ -to-Bell version of \widetilde{XX} , followed by a Bell-to- $|++\rangle$ version of \widetilde{ZZ} .

To characterize the encoded Hadamard gate, we performed Monte Carlo sampling with two-qubit depolarizing noise applied to every physical two-qubit gate in the circuit; measurements and feedforward were assumed ideal. For each sampled fault pattern, the induced Pauli error is propagated through the Clifford circuit, the run is postselected on the trivial stabilizer syndrome and on the ancillas returning to the expected final state, and the resulting logical action is compared with the ideal encoded Hadamard on the chosen logical qubit. One could also choose the opposite versions of the \widetilde{XX} and \widetilde{ZZ} gadgets, but then the final ancillas would need to be checked in the Bell basis rather than in the X basis.

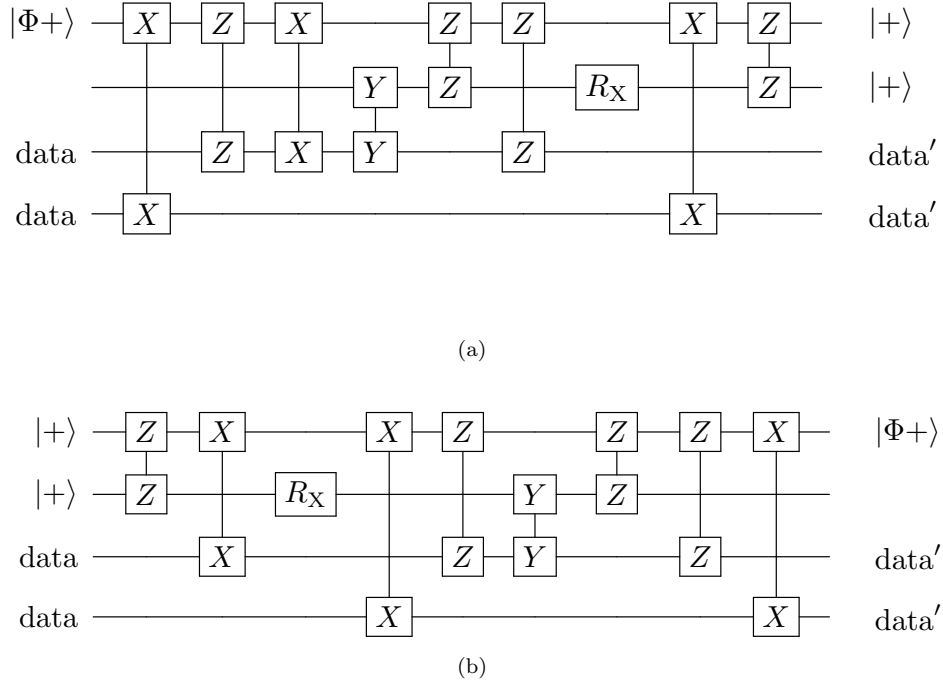
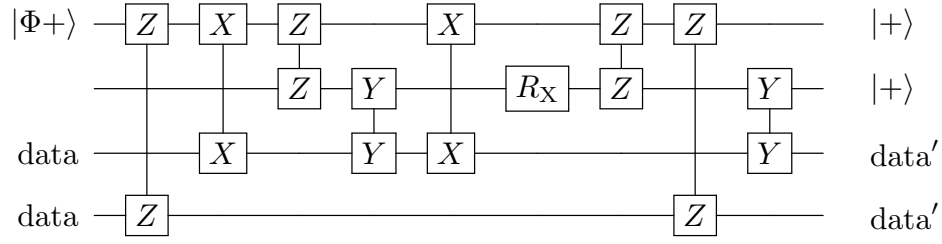
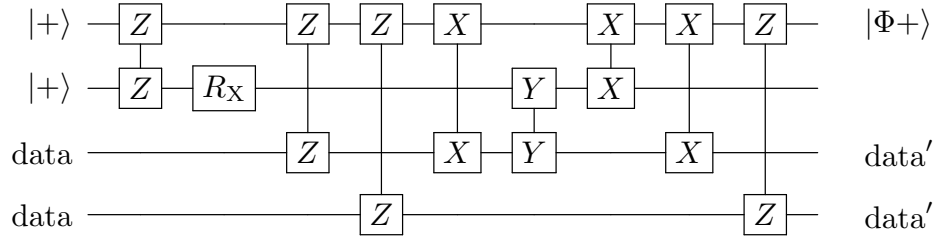


FIG. 9. Weakly fault-tolerant gadgets for the XX rotation. Panel (a) consumes a Bell pair and returns the ancillas in $|++\rangle$; panel (b) consumes $|++\rangle$ and returns a Bell pair. Alternating the two versions allows successive XX and ZZ gadgets to reuse ancillas without an explicit re-preparation step.



(a)



(b)

FIG. 10. Weakly fault-tolerant gadgets for the ZZ rotation. Panel (a) consumes a Bell pair and returns the ancillas in $|++\rangle$; panel (b) consumes $|++\rangle$ and returns a Bell pair.

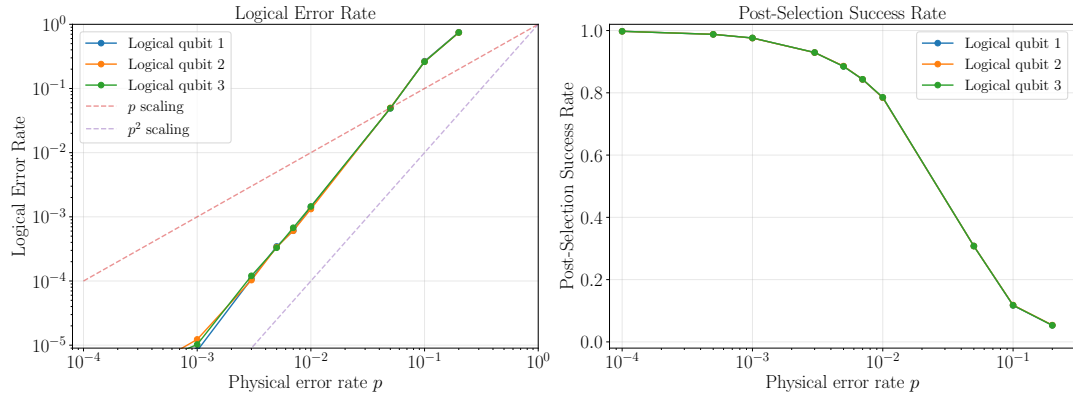


FIG. 11. Simulation results for the encoded Hadamard gate on the three logical qubits. In the low-noise regime, the postselected logical error rate is approximately quadratic in the physical two-qubit error rate, consistent with weak fault tolerance. The right panel shows the corresponding postselection success rate.

Appendix B: Fault-tolerant encoding circuits for both versions of the $[[8, 3, 2]]$ code

1. Version 1

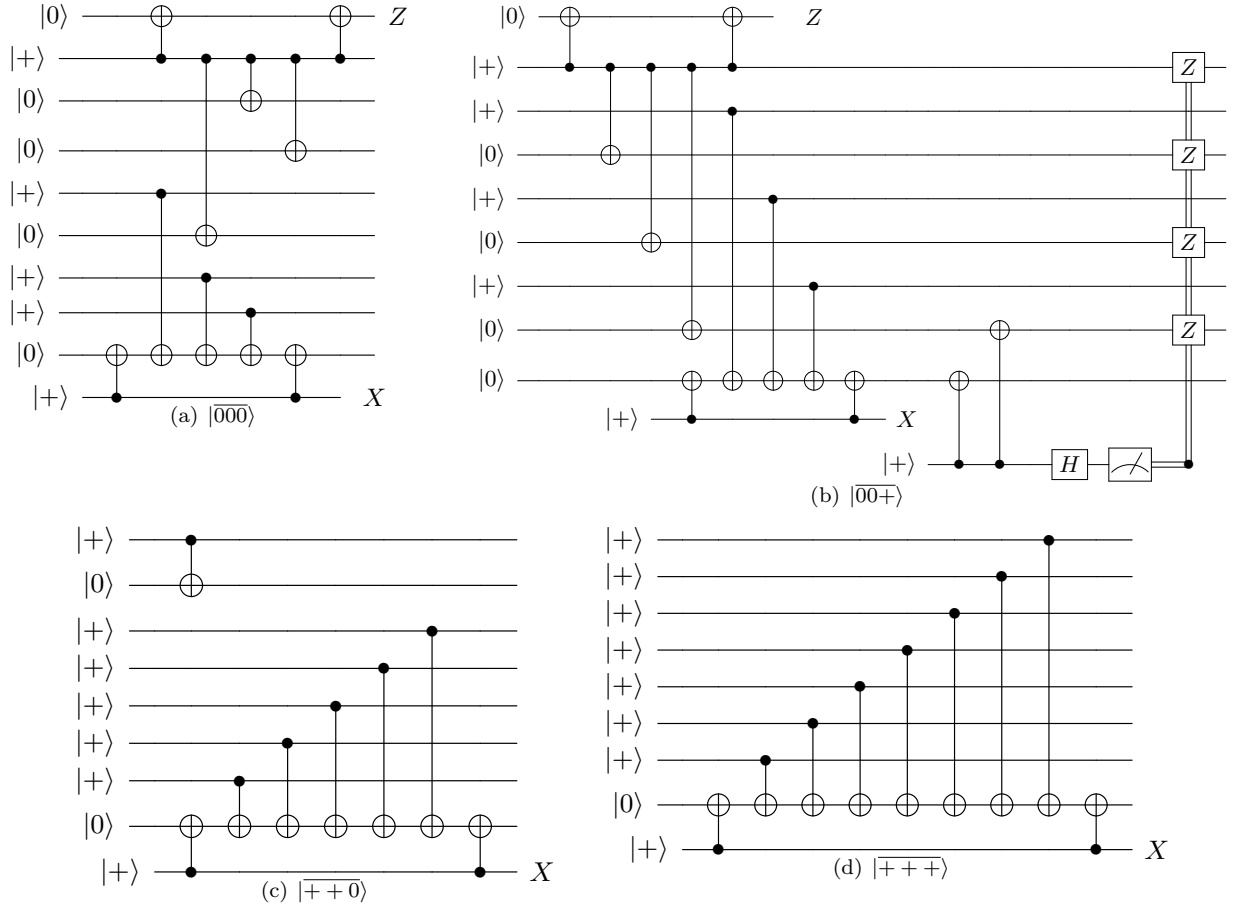


FIG. 12. Fault-tolerant state-preparation circuits for the Version 1 $[[8, 3, 2]]$ code: (a) $|000\rangle$, (b) $|00+\rangle$, (c) $|++0\rangle$, and (d) $|+++ \rangle$. Terminal X and Z labels on ancilla lines denote measurements in the corresponding basis. Boxes labeled X or Z connected by classical double lines denote feedforward Pauli corrections conditioned on the measured ancilla outcome.

2. Version 2

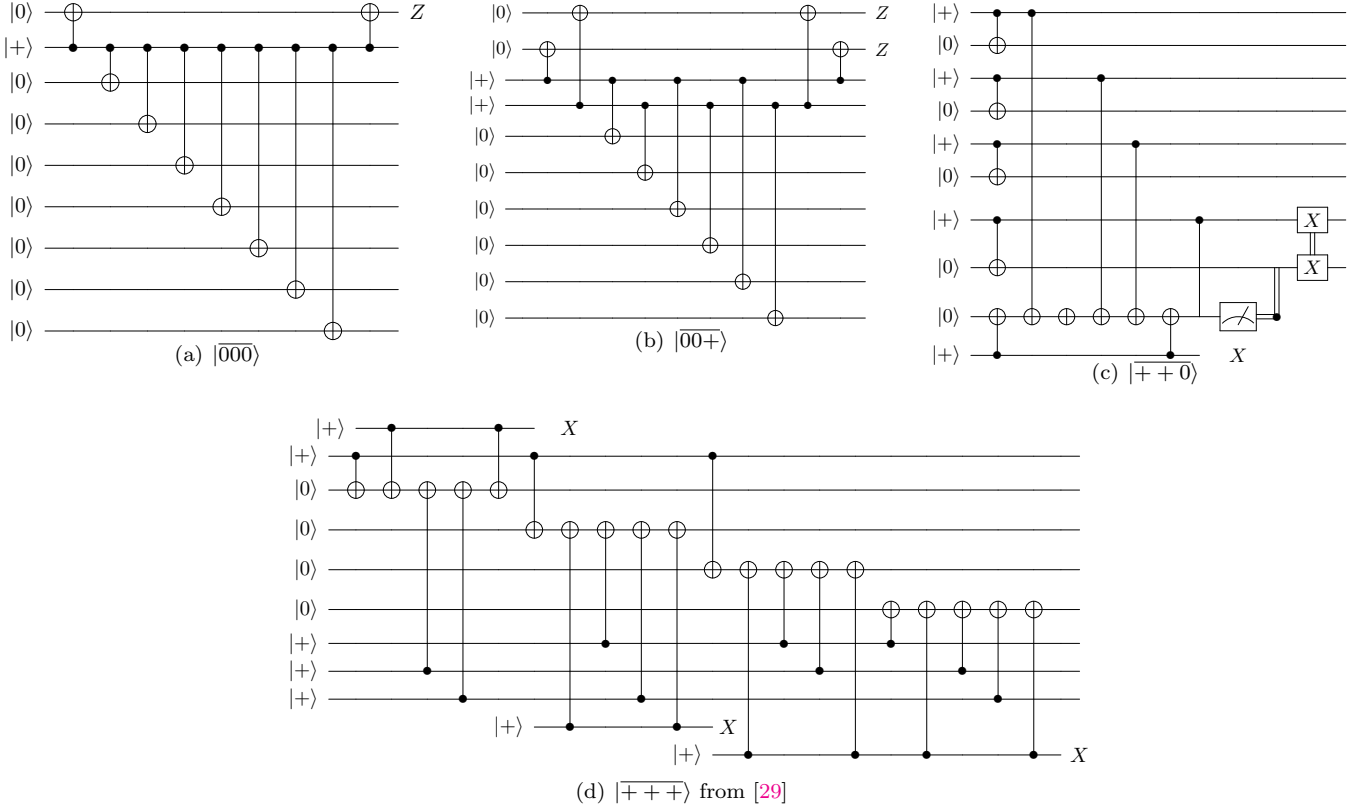


FIG. 13. Fault-tolerant state-preparation circuits for the Version 2 $[[8, 3, 2]]$ code: (a) $|000\rangle$, (b) $|00+\rangle$, (c) $|++0\rangle$, and (d) $|+++ \rangle$ (from Ref. [29]). Terminal X and Z labels on ancilla lines denote measurements in the corresponding basis. Boxes labeled X or Z connected by classical double lines denote feedforward Pauli corrections conditioned on the measured ancilla outcome.

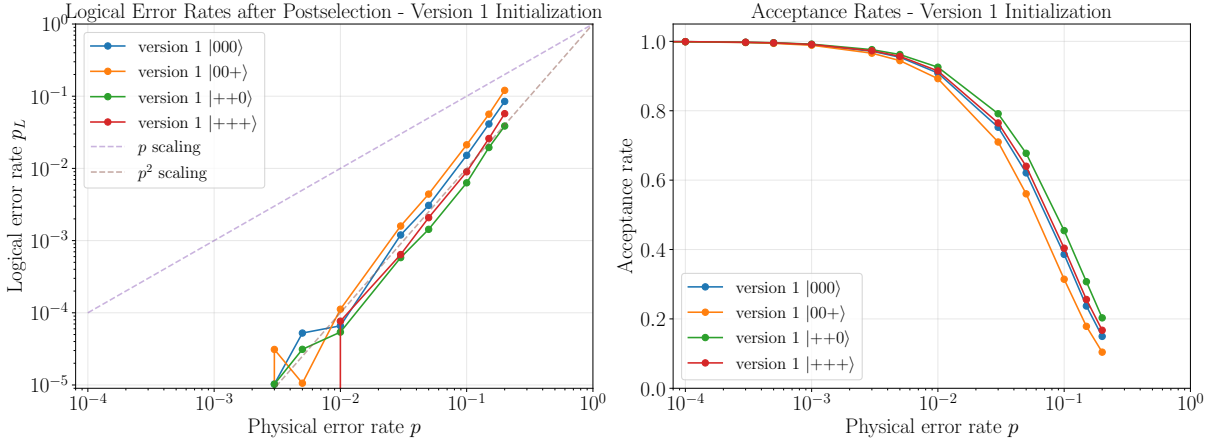


FIG. 14. Simulation results for the Version 1 state-preparation circuits in Fig. 12. We apply depolarizing noise with physical error rate p to every CNOT gate and report both the postselected logical error rate and the acceptance rate. The observed low-noise scaling is consistent with weak fault tolerance.

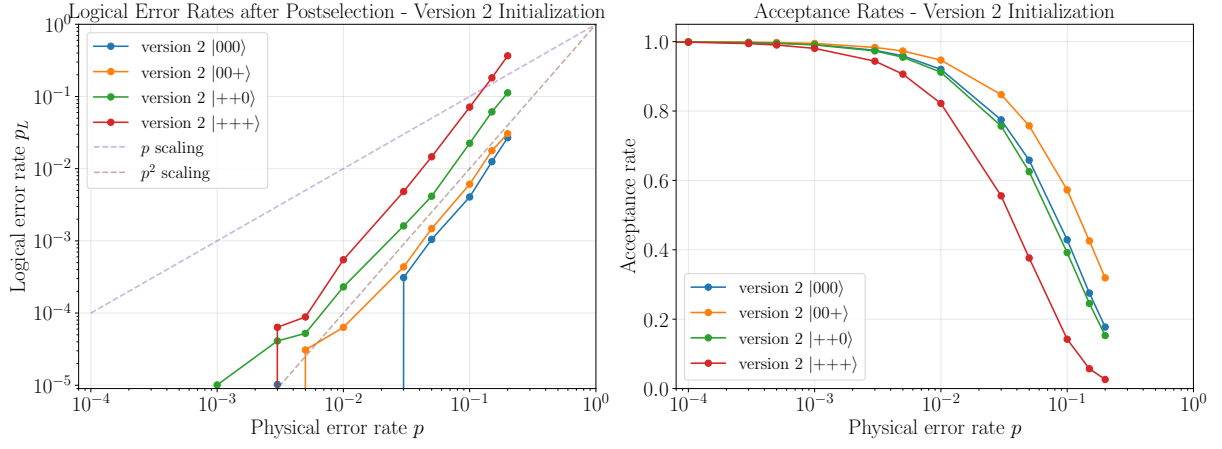


FIG. 15. Simulation results for the Version 2 state-preparation circuits in Fig. 13. We apply depolarizing noise with physical error rate p to every CNOT gate and report both the postselected logical error rate and the acceptance rate. The observed low-noise scaling is consistent with weak fault tolerance.

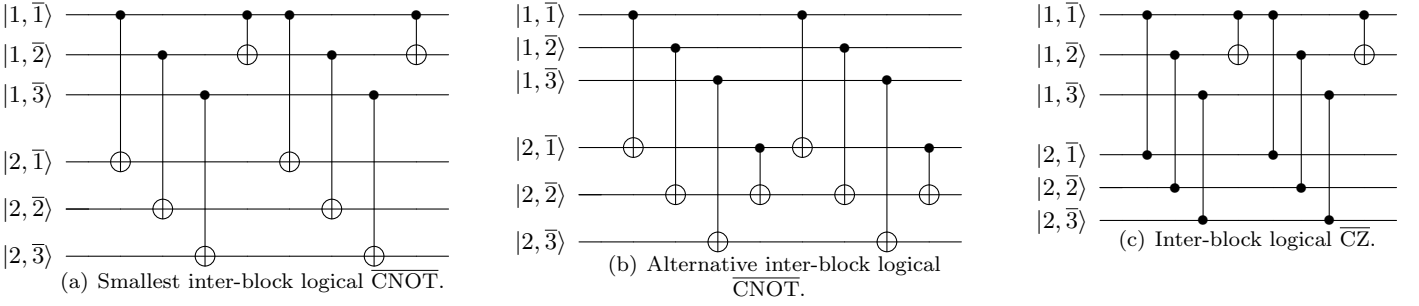


FIG. 16. Inter-block logical gates between blocks 1 and 2.

Appendix C: Extensions of the single inter-block logical $\overline{\text{CNOT}}$ gate

The logical $\overline{\text{SWAP}}$ gates in Fig. 3 are used only to move the target from $|2, \bar{2}\rangle$ to $|2, \bar{1}\rangle$; they are not required for the core construction. Removing them yields Fig. 16(a), which implements a single inter-block logical $\overline{\text{CNOT}}$ from logical qubit $\bar{1}$ of block 1 to logical qubit $\bar{2}$ of block 2.

More generally, two layers of parallel inter-block logical $\overline{\text{CNOT}}$ gates, separated by an in-block logical $\overline{\text{CNOT}}(\bar{i} \rightarrow \bar{j})$ on one block and followed by the same in-block gate again, cancel the unwanted pairwise couplings and leave only the desired single inter-block logical $\overline{\text{CNOT}}$ from logical qubit \bar{i} in one block to logical qubit \bar{j} in the other. In Fig. 16(a) the in-block gate is applied on block 1, whereas Fig. 16(b) shows the equivalent construction with the in-block gate applied on block 2. The latter form is useful when only one of the two blocks admits a convenient fault-tolerant in-block logical $\overline{\text{CNOT}}$ implementation.

The same cancellation idea also gives a single inter-block logical $\overline{\text{CZ}}$: replacing the two layers of parallel inter-block $\overline{\text{CNOT}}$ gates by layers of parallel inter-block $\overline{\text{CZ}}$ gates yields the construction shown in Fig. 16(c).